High Resolution Heterodyne 3D Imaging

Randy Reibel, Trent Jackson, Nathan Greenfield, Trenton Berg, David Kozicki, Eric Seger, Chris Wilson, and Peter Roos
Bridger Photonics Inc.
2310 University Way, Bldg. 4-4
United States
reibel@bridgerphotonics.com

1. Introduction

Conventional laser radar (ladar) imaging systems or 3D imagers follow two different design architectures, each of which typically use direct detection of traditional pulsed lasers. First, there are fully scanned systems which rely upon a mechanical spatial beam scanner synchronized with a pulsed laser system and a single fast photodetector. Recent advances in micro-electro-mechanical systems (MEMS) technology have made fast, compact and rugged beam scanners available. However, the time to complete a full scan to create an image is the primary drawback. [1] The main benefit for these systems is that the receive detector and the electronics for time-of-flight measurement only need to be replicated once.

The second approach, known as flash ladar, relies upon spreading the pulsed laser energy across the full FOV and placing fast detector arrays at the focal plane, so called fast focal plane arrays (FPAs). The advantage for flash ladar systems is that the FPA is used to collect both the cross-range and down-range content during a single pulse of the laser system, allowing the imager to capture an image nearly instantaneously with essentially no blur.[2]

Unfortunately, the use of pulsed laser sources in both these systems makes them unattractive for high resolution imaging applications because of bandwidth and digitizer limitations.

Hybrid systems, which incorporate scanning with lower dimensionality focal plane arrays, are getting increased attention. This is because the ability to scan some of the field-of-view can be traded against the cost and development of the FPA. Combining the hybrid concept with an FMCW ladar ranging approach is even more attractive because the bandwidth and digitizer requirements on the FPA are further reduced.[3] We describe our current efforts at constructing a hybrid 3D imaging system in this paper and highlight some of the advantages of this approach for atmospherically adverse conditions.

2. Background and Motivation

Bridger Photonics Inc. (Bridger) and Montana State University have pioneered the active stabilization and control of highly-power efficient, extremely broadband swept laser sources for FMCW ladar.[4,5] The advantages include: (a) their extreme sensitivity allowing low return light levels, (b) their capability to deliver extremely high down-range resolution using low-bandwidth receiver electronics (down-range resolution is inversely proportional to the sweep bandwidth), (c) their high power efficiencies and ability to capitalize on telecom amplifiers and (d) their compact, robust packaging.

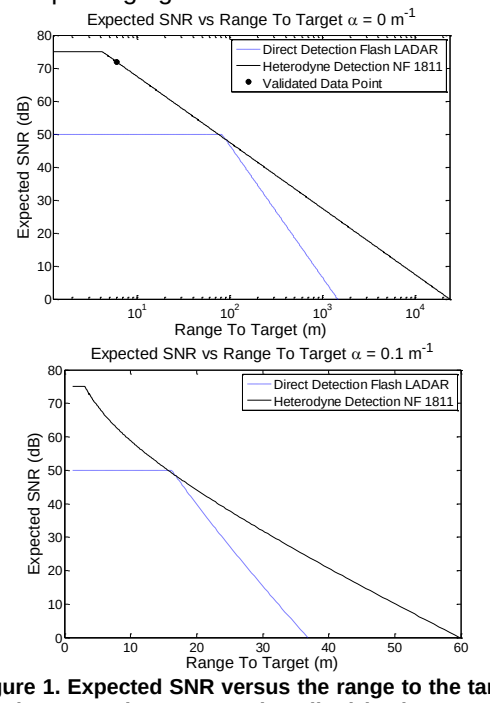

Figure 1. Expected SNR versus the range to the target for the DD and HD cases described in the text with (Top) no atmospheric attenuation and (Bottom) the atmospheric attenuation experienced during the Yuma Proving Ground tests. In both cases, the HD system is capable of seeing substantially further than the DD system.

One important difference between heterodyne detection (HD) systems and direct detection (DD) systems is their dependence upon the return power of the light from the

target. In a HD system, the detected voltage from the photodetector is $V_{DD} \propto P_{RX}$, where P_{RX} is the received power on the photodetector. In a DD ladar scheme the detected voltage is proportional the square root of the optical return power: $V_{HD} \propto \sqrt{P_{RX}}$. Figure 1 shows theoretical analysis for the expected SNR for a pulsed flash ladar system versus a hybrid 3D heterodyne imaging system. The HD system is modelled using specifications reported here and the DD system is similar to systems found in Reference [2] with both systems given as equivalent configurations as possible. The return power dependence leads to a slope drop off of 2 on a log-log plot for the DD system versus a slope of 1 on a log-log plot for the HD system when expected SNR is compared (see top plot in Figure 1). The cap on expected SNR shown for both cases is set by the maximum achievable dynamic range, which is often limited by digitizer performance. Because of this return power dependence, the impact of extinction due to atmospheric attenuation is also more sever. For example, the DD system has an $SNR_{DD} \propto e^{-4\alpha R}$, whereas the HD system has an $SNR_{HD} \propto e^{-2\alpha R}$, where α is the atmospheric extinction coefficient. This leads to better penetration capabilities for HD into smoke, fog, or brownout conditions than traditional flash ladar system as shown in the bottom of Figure 1.

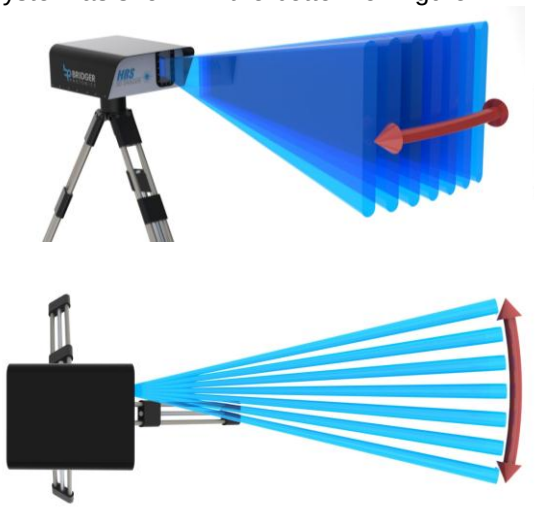

Figure 2. (Top) A view of the 3D imager and the output beam. Information imaged in elevation via a one dimensional focal plane array and in azimuth via a proprietary non-mechanical scanning method and in downrange via FMCW ladar resulting in a true angle-angle-range image. (Bottom) A view from the top showing the azimuth scan angle.

The primary drawback to heterodyne imaging systems is that they are sensitive to Doppler effects and these effects can be quite substantial at optical wavelengths. However, such Doppler effects can also be a benefit, especially for penetrating brownout conditions. DD systems are known to be prone to severe clutter when probing through a brownout cloud due to strong returns from the cloud. In HD systems, the Doppler effects from the cloud returns are strongly Doppler broadened, leading to a significant reduction in false alarms and clutter from the sand cloud.

3. System Design

Heterodyne 3D imaging has been performed experimentally before with some success.[6] Bridger's primary approach to creating a heterodyne imager relies on a hybrid approach that utilizes a lower dimensional FPA. Figure 2 shows the approach using Bridger's 3D Imager. Laser light from a stabilized laser source is reshaped by transmitter optics into an elliptical beam, which is then non-mechanically scanned using proprietary techniques across the scene. Light reflected from the target is imaged onto a detector array by the receiver optics and the range is detected using FMCW heterodyne detection. The detected signals are processed to form point clouds and are displayed using a computer. This system was used to take all of the data in this paper (except for Figure 3) and had a 10 W transmit power with a 3 degree field-of-view.

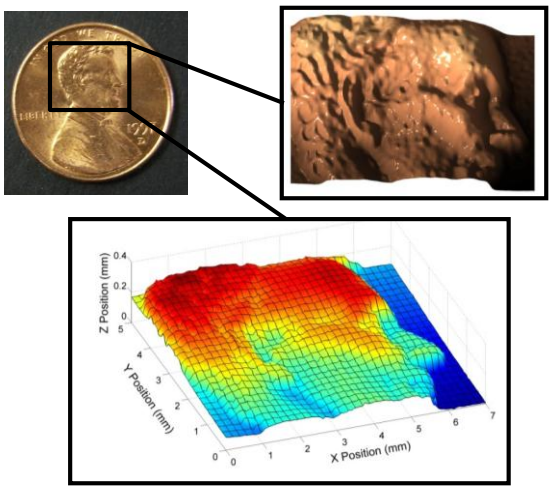

Figure 3. (Top Left) The approximate location of the scanned section for a U.S. Penny. (Top Right and Bottom) Renderings of the three dimensional imagery acquired with the swept source.

4. Demonstrations

To demonstrate the capability of Bridger's ultra-high-resolution heterodyne imaging capabilities, first a U.S. penny was set up on a 2D translation stage. An effective delay of 1 m was created to the target and a single down-range capture was made per scan point. The range to the surface of the penny was then estimated from the range profile and a point cloud formed. Figure 3 shows the results for 3D renderings of the measured data. The upper left conventional image shows the approximate location of the scan. The image in the upper right was a 3D shadowed rendering of the data showing that very fine surface structure is apparent. The lower 3D

plot shows the surface height as a function of color and provides a scale. From this plot, the features on Lincoln's face are measured to be a few hundred microns in height. This proof-of-concept demonstration showed that actively stabilized laser sources could be utilized for 3D heterodyne imaging.

To explore the benefit of the imager in brownout conditions, tests were conducted in a brownout chamber (see acknowledgements). The brownout chamber was approximately 10 m long and dust similar to that found in Iraq or Afghanistan was circulated through the chamber. Two optical windows on the chamber allowed the laser light to pass through the test brownout condition. By adding various known weights of sand and knowing the volume of the brownout chamber, an upper limit for the sand density could be determined.

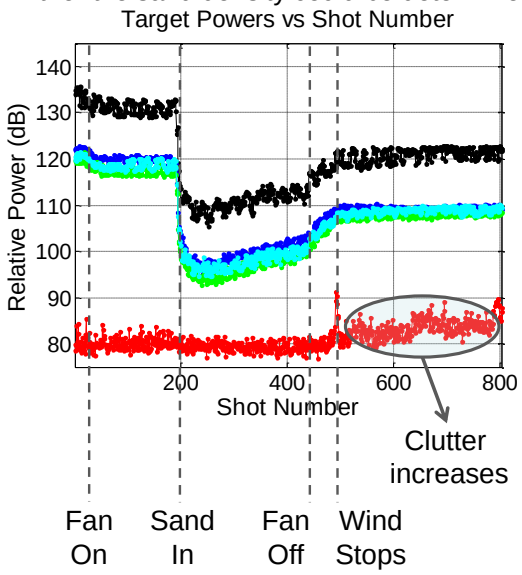

Figure 4. Time resolved return powers from various targets along with the noise floor (see text).

Figure 4 shows the range resolved relative return powers from various target types (black - specular reflector, blue and green – wood, cyan – plastic, red – noise floor) versus the pulse number or time for a maximum sand density of about 9000 mg/m^3. Note that the actual targets were placed about 15 m beyond the end of the brownout chamber resulting in a total distance to the targets of about 25 m. The actual sand density in the chamber is likely reduced by almost an order of magnitude but there was no method to calibrate the density in these measurements and so the upper maximum density is used. When wind in the chamber is initially turned on, a slight decrease in signal is observed, likely due to some leftover contaminants within the chamber. When the sand is poured into the windy chamber (around shot 200) a dramatic reduction in signal strength is observed across targets. The attenuation peaks around shot 250 and slowly diminishes likely due to heavier particulates dropping out from circulation. Around shot number 450 the fans are turned off and the heavier particles drop from the air quickly. Once the wind speeds completely stop (near shot 500), only the lightest particles remain in the air resulting in a weaker brownout condition that lingers for a long time.

By examining the noise floor, one notices that there is next to no clutter resulting from the presence of the brownout cloud. This is a result of the strong Doppler broadening from the moving sand particles making their range returns lower than the noise floor. However, as the wind speed stops, the clutter inreases, meaning that the Doppler broadening on the sand particles is reduced to the point that they can be easily measured. Figure 5 shows the resulting sand particle distribution that was imaged with the system (using a down-range resolution of about 2 cm). This image shows a 2D slice of the imager (down-range and one cross-range dimension) with color representing the return power strength in decibels. Wisps from the sand cloud are now apparent. These particles disappear when the fans for the brownout chamber are turned on demonstrating that clutter rejection during brownout penetration is an inherent feature of this heterodyne imager. This image also serves to highlight the high-resolution capabilities of Bridger's system. Note that resolution as referred to here is the half-width of the range peak and is around a factor of 30 better than competing flash ladar approaches.

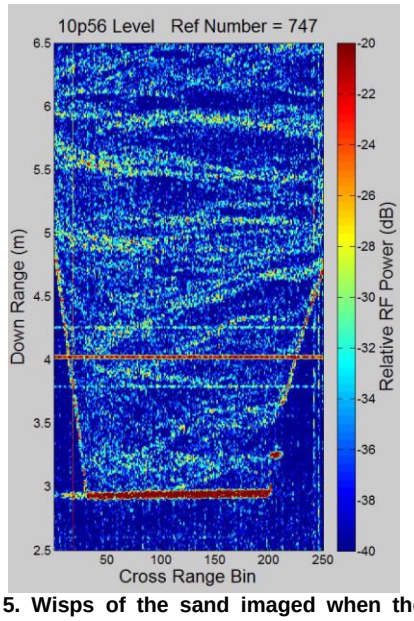

Figure 5. Wisps of the sand imaged when the wind velocity is dropped nearly to zero in the sand chamber. The front of the chamber is visible near 3 m and the side walls are diagonal lines stretching upwards. The signal at 4 m is a noise spur.

Figure 6 (Top) shows the measured system SNR during the peak attenuation for the targets versus the chamber's upper limit "maximum" possible sand density. As can be seen, strong SNRs exist even out to beyond

the 12000 mg/m^3 point (again we remind the reader that the actual sand density in the chamber is likely an order of magnitude less as described above). Figure 6 (bottom) shows the measured extinction coefficient from the specular reflection. Bridger has previously estimated from publicly available Sandblaster data, that helicopter brownouts can have extinction coefficients of 0.05 to 0.25 per meter and possibly higher for telecom wavelengths.[7] This would suggest that Bridger's imager could image through about 10 m of 0.25 per meter extinction and still have upwards of 40 dB SNR off of diffuse targets.

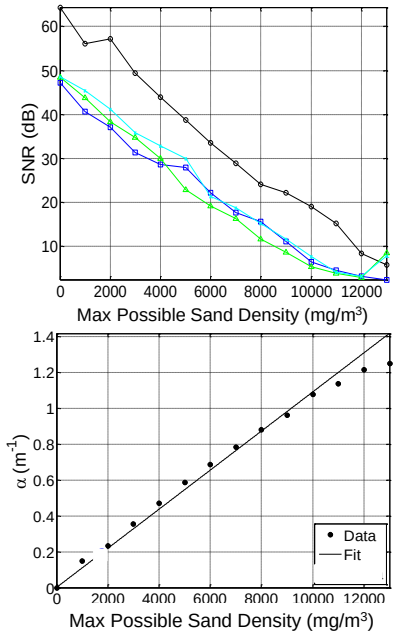

Figure 6. (Top) The minimum SNR seen versus maximum possible sand density supported by the brownout chamber. See text for target coloring which is the same as Figure 4. (Bottom) The measured extinction coefficient.

Finally, a 3D image is shown in Figure 7 (bottom) of a scene similar to the one in Figure 7 (top). Different targets are identified. In the 3D imaged scene, a wooden target (Wd) is near the center of the scene with a specular reflector on it (Sp). Extension cords and ropes were used to make small, thin obstacles (Wr 1, Wr 2). Aluminum tubing was used to make large specular targets (C1, C2, C3, C4). The back wall was made of a tarp (near down range 35 m). This shows that the system is capable of making 3D images of real scenes.

5. Conclusions

In this paper we have described the many advantages of a heterodyne imaging system. These benefits include: 1) ultra-high sensitivity to return light, 2) high range resolutions, 3) affordable, high average transmit powers, 4) the capability to range further into atmospherically adverse conditions as compared to direct detection systems. The drawbacks to such imagers is possible blurring or range errors due to Doppler effects.

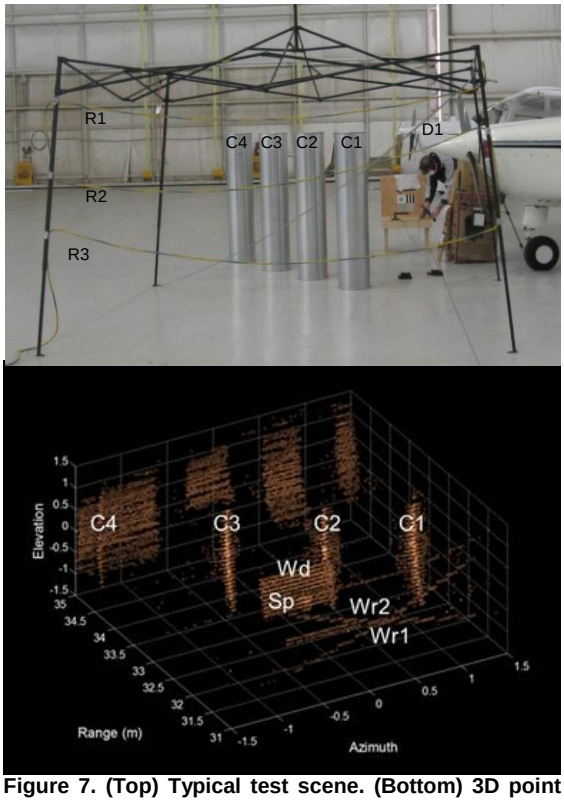

Figure 7. (Top) Typical test scene. (Bottom) 3D point cloud obtained from ~35 m using Bridger's system.

6. Acknowledgements

The authors would like to acknowledge ITT Geospatial Systems, esp. Chris Rodgers, Jarett Bartholomew, and Andrew Hsu for building, operating and supporting tests using the brownout chamber. We thank Dave Ludwig at the Office of Naval Research for helpful discussions regarding rotorcraft. The authors would like to thank Wally Buell and Steve Beck of Aerospace Corp. for helpful discussions about heterodyne detection ladar and adverse atmospheric conditions.

7. References

[1] J. P. Siepmann and A. Rybaltowski, "Integrable Ultra-Compact, High-Resolution, Real-Time MEMS Ladar for the Individual Soldier," IEEE MILCOM 2005, pp. 3073-79 (2005).
[2] See for example http://www.advancedscientificconcepts.com/
[3] B. Krause, P. Gatt, C. Embry, and J. Buck, "High-Resolution 3D Coherent Laser Radar Imaging," Laser Radar Technology and Applications XI, edited by G. W. Kamerman, M. D. Turner, Proc. of SPIE Vol. 6214, 62140V, (2006).
[4] P. A. Roos, R. R. Reibel, B. Kaylor, T. Berg, Z. W. Barber, and W. R. Babbitt, "Ultra-broadband optical chirp linearization for precision metrological applications," *Optics Letters*, vol. 34, pp. 3692–3694, 2009;
[5] Z. W. Barber, W. R. Babbitt, B. Kaylor, R. R. Reibel, and P. A. Roos, "Accuracy of active chirp linearization for broadband frequency modulated continuous wave ladar," *Applied Optics*, vol. 49, pp. 213–219, 2010
[6] G. Pearson, K. Ridley and D. Willete, "Chirp-pulse-compression three-dimensional lidar imager," Appl. Opt. 44 pp. 257-65 (2005).
[7] Sandblaster 2 Task 5 Final Technical Report, MRI Project No. 110565.1.001, Midwest Research Institute, October 31, 2007.